Evidence for Langmuir Envelope Solitons in Solar Type III Burst Source Regions

G. Thejappa[1], M. L. Goldstein[2], R. J. MacDowall[2], K. Papadopoulos[1] and R. G. Stone[2]
[1]Department of Astronomy, University of Maryland, College Park, MD 20742,

USA[2]NASA, Goddard Space Flight Center, Greenbelt, MD 20771, USA,

Short title:

Abstract. We present observational evidence for the generation of Langmuir envelope solitons in the source regions of solar type III radio bursts. The solitons appear to be formed by electron beams which excite either the modulational instability or oscillating two-stream instability (OTSI). Millisecond data from the Ulysses Unified Radio and Plasma Wave Experiment (URAP) show that Langmuir waves associated with type III bursts occur as broad intense peaks with time scales ranging from 15 to 90 milliseconds (6 – 27 km). These broad field structures have the properties expected of Langmuir envelope solitons, *viz.*: the normalized peak energy densities, $W_L/n_eT_e \sim 10^{-5}$, are well above the modulational instability threshold; the spatial scales, L, which range from 1 – 5 Langmuir wavelengths, show a high degree of inverse correlation with $(W_L/n_eT_e)^{1/2}$; and the observed widths of these broad peaks agree well with the predicted widths of envelope solitons. We show that the orientation of the Langmuir field structures is random with respect to the ambient magnetic field, indicating that they are probably isotropic structures that have evolved from initially pancake-like solitons. These observations suggest that strong turbulence processes, such as the modulational instability or the OTSI, stabilize the electron beams that produce type III bursts.

1. Introduction

The production of solar type III radio emission involves the generation of high levels of Langmuir waves and their subsequent conversion into electromagnetic radiation at f_{pe} and $2f_{pe}$ ($f_{pe} = (n_e e^2/\pi m_e)^{1/2}$ is the electron plasma frequency, where e, n_e, and m_e are the electron charge, number density, and mass, respectively). Electron beams propagating outward from the sun amplify Langmuir waves through the bump-on-tail instability [*Bohm and Gross*, 1949] at the resonant frequency $\omega_L = k_L v_b$, where k_L is the wave number of the Langmuir wave, v_b is the speed of the electron beam, $\omega_L^2 = \omega_{pe}^2 + 3k_L^2 v_{Te}^2$, $\omega_{pe} = 2\pi f_{pe}$, and v_{Te} is the electron thermal speed. Early theoretical models describing the injection of electron beams into the solar atmosphere predicted that excitation of Langmuir waves would extract all the streaming energy from the electrons within 100 km or less [*Sturrock*, 1964; *Tsytovich*, 1970], whereas *in situ* detection of type III burst associated Langmuir waves and electron beams [*Lin et al.*, 1986; *Kellogg et al.*, 1992; *Reiner, Fainberg and Stone*, 1992; *Thejappa et al.*, 1993a,b; *Thejappa, Wentzel and Stone*, 1995; *Thejappa, Stone and Goldstein*, 1996; *Thejappa and MacDowall*, 1998] indicate that the electron beams reach 1 Astronomical Unit (AU) or more. Consequently, the beam cannot be in continuous resonance with Langmuir waves while propagating from the corona to and beyond 1 AU. Some process must remove Langmuir waves from resonance with the beam by, for example, reducing k_L through weak turbulence processes, such as induced scattering or electrostatic decay [see, *Kaplan and Tsytovich*, 1973] or by increasing k_L through strong turbulence processes such as the modulational instability or oscillating-two-stream instability (OTSI) [*Papadopoulos, Goldstein and Smith*, 1974; *Smith, Goldstein and Papadopoulos*, 1979; *Goldstein, Smith, and Papadopoulos*, 1979].

Beam stabilization occurs via weak turbulence processes, when the rate of removal of Langmuir waves from resonance with the beam exceeds the growth rate of the instability. In contrast, the wavepackets generated by strong turbulence exert a

ponderomotive force on the plasma, making it spatially inhomogeneous, thus causing a loss of coherence and decoupling the wavepacket and beam. In the first application of strong turbulence theory to the type III burst problem, *Papadopoulos, Goldstein and Smith* [1974] used the term oscillating two stream instability, or OTSI, to describe the initial strong turbulence processes that form the small-scale soliton-like structures. During later stages of evolution, these solitons collapse [*Zakharov* 1972; *Nicholson et al.* 1978; *Kellogg et al.* 1992; *Shapiro and Shevchenko*, 1984; *Robinson* 1997].

The linear regime of the OTSI or modulational instability is characterized by the formation of an envelope soliton which is the envelope of the high frequency Langmuir waves trapped inside a self-generated density cavity. The envelope soliton is also referred to as an oscillating soliton [*Kuznetsov, Rubenchik and Zakharov*, 1986], because it contains oscillations of definite frequency and wavelength. The size of the envelope soliton, which ranges from 1 to several Langmuir wavelengths is determined by the peak intensity of the trapped waves: the higher the field strength, the narrower the width.

In previous studies, we evaluated the emission mechanisms at f_{pe} [*Thejappa et al.*, 1993a,b] and at $2f_{pe}$ [*Thejappa, Stone and Goldstein*, 1996] using *in situ* wave data associated with several type III bursts from the Unified Radio and Plasma Wave Experiment (URAP) on Ulysses. Our main emphasis in those studies was to evaluate various type III emission mechanisms. In the present paper, we reanalyze the high resolution observations of Langmuir waves that occur as the broad intense field structures with durations ranging from 15 to 90 milliseconds. We argue that these field structures are probably quasi-stable Langmuir envelope solitons generated by the modulational instability. Our conclusion is based on the fact that the peak intensities are well above the modulational instability thresholds, the spatial scales ($1-5$ Langmuir wavelengths, λ_L) are consistent with the widths computed for envelope solitons, and, most importantly, the widths of these envelopes vary inversely with their peak intensities.

For most of the Langmuir wave broad peaks, the normalized energy densities $W_L/(n_e T_e)$ are slightly less than or equal to the corresponding values of Ω_e^2/ω_{pe}^2, where $\Omega_e = eB/(m_e c)$ is the electron cyclotron frequency. A careful examination of the data has revealed that the ambient magnetic field $\vec{B}$ is oriented randomly with respect to the antenna direction, which is the probable direction of the high resolution events of Langmuir wave field structures. This implies that even though magnetized Langmuir waves initially form pancake-like structures with transverse spatial scales $S_\perp$ much larger than the longitudinal ones (S), i.e., $S_\perp \gg S$, they evolve into more isotropic structures with $S_\perp \sim S$. This isotropization occurs because the perpendicular spatial scales decrease more rapidly than do the parallel spatial scales so long as the inequality $k_L^2 \lambda_D^2 < \Omega_e^2/\omega_{pe}^2$ holds [*Krasnoselskikh and Sotnikov*, 1977]. We also show observations of weak spectral enhancements of ion acoustic waves at about $\sim$ 100 Hz in association with the envelope solitons. We discuss the implications of these observations for the stabilization of the electron beams that excite type III radio bursts.

In section 2, we present the observations. Section 3 contains a solution of Zakharov's equation (unmagnetized case) in the form of an envelope soliton and compares it with observations. The magnetized Langmuir waves are shown to form planar solitons that evolve into isotropic solitons and eventually collapse. In section 4, we discuss the implications of these observations for type III burst beam stabilization and the possible coexistence of electrostatic decay with modulational instabilities. In section 5, we present the conclusions.

2. Observations

We concentrate primarily on three local type III events and their associated *in situ* waves, observed by the URAP experiment on 11 December 1990, 22 February 1991 (identified by *Reiner, Fainberg and Stone*, [1992]), and 7 March 1991 (identified by *Thejappa et al.*, [1993a]). In addition to a variety of wave data from the Radio

Astronomy Receiver (RAR), the Plasma Frequency Receiver (PFR), the Wave Form Analyzer (WFA), and the Fast Envelope Sampler (FES) of the URAP experiment [*Stone et al.*, 1992], we use magnetic field (B) data from the fluxgate magnetometer [*Balogh et al.*, 1992], and the electron density (n_e), electron temperature (T_e), ion temperature (T_i), and solar wind speed (V_{sw}) data from the Solar Wind Plasma Experiment SWOOPS [*Bame et al.*, 1992]. These data were provided by the National Space Science Data Center (NSSDC).

In columns 1, 2 and 3 of Figure 1, we present the peak electric field signals corresponding to local type III events of December 11, February 22 and March 7, respectively. The first and second rows show the time profiles of the type III bursts at $\sim 2f_{pe}$ and $\sim f_{pe}$, respectively, whereas the bottom row shows the corresponding Langmuir wave electric field signals. It is clear from this figure that the type III burst time profiles are generally characterized by a steep rise followed by a smooth and slow decay. Since the second harmonic emissions do not have exactly the same time development as that of fundamental emissions, it is very likely that the high frequency electromagnetic emission contains the first as well as the second harmonics. It is clear from the bottom row that the Langmuir wave electric fields are very bursty in nature. Their peak amplitudes are 3 to 4 orders of magnitude larger than the respective type III burst electric field amplitudes. The type III burst electric field measurements are from the RAR with a time resolution of $\sim$ 128s and a high sensitivity of $\sim 30 \mathrm{nVHz}^{-1/2}$ at 10 kHz. The Langmuir wave data are from the PFR with a time resolution of $\sim$ 16s (maximum value in 16 s windows) and a rms sensitivity of $\sim 100 \mathrm{nVHz}^{-1/2}$ at 10 kHz. It is clear from this figure that the intense Langmuir wave activity coincides with the peak of the type III burst emission. In Table 1, we list all relevant solar wind parameters, such as the electron density, n_e; the electron temperature, T_e; the ion temperature, T_i; the solar wind speed, V_{sw}, and the magnetic field, B.

Figures 2a, b, and c show the high time resolution snapshots of Langmuir wave

electric field envelopes associated with the type III bursts of December 11, 1990, February 22, 1991, and March 7, 1991, respectively. These data are obtained by the FES, which is capable of resolving the field structures with time scales as small as one millisecond (for a detailed description of the instrument, [see *Kellogg et al.*, 1992; *Theissen and Kellogg*, 1993]. As seen in Figure 2, the Langmuir wave events show random fluctuations in the beginning and a broad intense peak in the middle, after $\sim$ 500 milliseconds. Step-like structures are often present during the rising phase of these broad peaks. The asymmetric shapes and enhanced noise levels during the decay phase of these events are due to the 32-dB attenuator, activated by the intense central peak (but *cf.* panel b). The role of the attenuator is to extend the dynamic range of the system, i.e., whenever the signal rises to saturation, the attenuator is switched into the signal stream, which remains connected for the remainder of the event cycle.

We have examined the orientation of the solar wind magnetic fields with respect to the X-antenna. During most of these FES events, the magnetic field is oriented randomly with respect to the X-antenna. Because the FES captures the most intense signals during each 30 minute interval, the observed events probably the electric field structures aligned along the antenna direction. This suggests that the Langmuir wave electric field signals of this study are also oriented randomly with respect to the magnetic field which implies that the Langmuir envelopes are approximately isotropic. In Table 2, we present the summary of these high time resolution observations. These include: (1) the peak electric field intensities of the broad central field structures, E_L, (2) the normalized Langmuir wave peak energy densities, $W_L/(n_e T_e) = \epsilon_0 E_L^2/(2n_e T_e)$ (ϵ_0 is the dielectric permittivity of the free space), (3) the measured 0.2-power duration of broad peak, ($t_{0.2}$) in units of milliseconds, (4) the 0.2-power widths of the broad peaks, $L_{0.2} = t_{0.2} V_{sw}$, and (5) the predicted 0.2-power widths of envelope solitons $S_{0.2}$ calculated using the observed ($\frac{W_L}{n_e T_e}$) and λ_D (see, section. 3).

In Figure 3, the plot of the 0.2-power widths of the broad FES peaks, $L_{0.2}$, versus

the square root of the corresponding inverse normalized energy densities, $[(n_e T_e)/W_L]^{1/2}$ is presented. As seen from this figure, $L_{0.2}$ increases with $[(n_e T_e)/W_L]^{1/2}$, implying that the more intense the peak, the narrower the width. We compute the correlation coefficient in this case as ~ 0.9. Such an excellent correlation indicates that these observed field structures most probably correspond to Langmuir wave fields trapped inside self-generated density cavities.

In Figures 4a, b and c, we plot the low frequency electric field spectra observed by the WFA in the frequency range $0 - 448$ Hz, as well as high frequency electric field spectra observed by the PFR ($0.57 - 35$ kHz), during 1- or 2-minute intervals containing the times of the FES events. The dotted lines correspond to the instrumental threshold of WFA. The prominent spectral peaks at ~ 10 kHz correspond to Langmuir waves, and weak spectral enhancements at ~ 100 Hz correspond to ion acoustic waves.

In the following sections, we examine whether the prominent broad central peaks are quasi-stable Langmuir envelope solitons and discuss their possible generation mechanisms. We discuss briefly whether the observed electric field spectral enhancements at low frequencies during the intense Langmuir wave envelopes are due to the coexistence of the electrostatic decay (weak turbulence) and modulational instability (strong turbulence) processes in some of the type III burst source regions.

3. Modulational Instability and Langmuir Envelope Solitons

Neglecting the magnetic field, the dispersion relation of Langmuir waves can be written as:

$$\omega_L^2 = \omega_{p_e}^2 + 3k_L^2 v_{T_e}^2, \qquad (1)$$

where v_{T_e} is the electron thermal speed. Whether the beam excited Langmuir wave packets broaden due to dispersion (weak turbulence processes), or, shrink due to ponderomotive effects, is determined by a threshold (neglecting dissipation) [*Sagdeev*,

1979; *Shapiro and Shevchenko*, 1984]:

$$\frac{W_{th}}{n_e T_e} \sim 3(\Delta k_L \lambda_D)^2, \tag{2}$$

where Δk_L is the average spread in wave numbers of the Langmuir wave packet. This is related to the typical values of the velocity dispersion in the beam, Δv_b, and the observed number of linear growth times, N, of Langmuir waves before onset of the modulational instability as [*cf. Lin et al.* 1986]:

$$\frac{\Delta k_L}{k_L} = \frac{\Delta v_b}{v_b} \frac{\ln 2}{2N}. \tag{3}$$

N, the number of linear growth times can be estimated from $N \simeq \ln p$, where p is ratio of the peak electric field amplitude of the broad peak (Figure 2) to the thermal background which is approximately an order of magnitude lower than the instrumental background. Here, we note that no self-consistent procedure is available for incorporating the collisionless dissipation in the threshold criterion (2), however, it is most likely that the dissipation processes slightly increase the modulational instability thresholds in comparison to those estimates obtained from Eqn (2). In the present case, the observed ratio of $p \sim 10^3$ corresponds to $N \sim 7$. So, for $\Delta v_b/v_b \simeq 0.15$ [*Lin et al.* 1986] and $N \sim 7$, we obtain $\Delta k_L/k_L \simeq 7 \times 10^{-3}$. For typical beam speeds, $v_b \sim 6 \times 10^7$ ms^{-1} [*Ergun et al.*, 1998], and the observed values of the electron plasma frequencies f_{pe} (Table 1), we obtain $k_L \sim \omega_{pe}/v_b \sim 1.2 \times 10^{-3}$ m^{-1}, $\sim 1.1 \times 10^{-3}$ m^{-1} and $\sim 1.1 \times 10^{-3}$ m^{-1}, for the December 11, February 22, and March 7 type III events, respectively. The corresponding wavelengths are $\lambda_L \sim 2\pi/k_L \sim 5$, 5.7 and 5.7 km. Using the estimated values of $\Delta k_L/k_L \simeq 7 \times 10^{-3}$, we find $\Delta k_L \sim 8.4 \times 10^{-6}$ m^{-1}, $\sim 7.7 \times 10^{-6}$ m^{-1}, $\sim 7.7 \times 10^{-6}$ m^{-1} for the three events. The observed values of Debye lengths (λ_D) corresponding to these events are 17, 17 and 13 meters (see, Table 1). By using these values of Δk_L and λ_D, the modulational instability threshold $W_{th}/(n_e T_e)$ is estimated as $\sim 6 \times 10^{-8}$, 5×10^{-8} and 5×10^{-8} for the three events. Here, we note that the initial

beam excited Langmuir wave numbers are $k_L\lambda_D < (m_e/m_i)^{1/2}$, and the corresponding group speeds are $V_g = 3(k_L\lambda_D)v_{Te} \sim (0.04 - 0.06)V_{Te} \sim c_s$, where m_e and m_i are the electron and ion masses, and V_{Te} and c_s are the electron thermal speed and ion acoustic speed, respectively.

From Table 2, it is clear that the observed normalized peak energy densities $W_L/(n_eT_e)$ significantly exceed the modulational instability thresholds. This implies that the ponderomotive force effects that drive the modulational instability are stronger than dispersive effects. The ponderomotive force arises from spatial gradients in wave intensity which affects both electrons and ions equally causing them to move toward the intensity minima, thus forming a ripple, δn_e, in the plasma density. The waves get trapped in those regions where the density is low because, from the Langmuir wave dispersion relation, waves with large k_L exist only where ω_{pe} is small. The wave trapping further enhances the intensity in the regions where it was already high, thus causing a ripple in the envelope to grow. For the modulational instability to occur, it is essential that the nonlinear frequency shift $\delta\omega_L$, responsible for the shrinkage of the wave packet, should have a sign opposite that of the group dispersion dv_g/dk_L which tends to spread the wave packet. Thus, after the modulational instability has grown somewhat, the Langmuir wave electric fields in real space consist of wave packets with group speeds less than $\sim c_s$. These wave packets will begin evolving into a series of Langmuir envelope solitons with group speeds less than $\sim c_s$ [*Degtyarev, Nakhan'kov and Rudakov*, 1974; *Nicholson et al.*, 1978].

3.1 Envelope Solitons in an Unmagnetized Plasma

The set of equations describing the modulational instability processes, which include envelope soliton formation are the well-known Zakharov equations [*Zakharov*, 1972], which, in one dimension, take the form

$$i\frac{\partial E}{\partial \tau} + \frac{\partial^2 E}{\partial z^2} = nE \tag{4}$$

$$\frac{\partial^2 n}{\partial \tau^2} - \frac{\partial^2 n}{\partial z^2} = \frac{\partial^2 |E^2|}{\partial z^2}. \tag{5}$$

Here we use the dimensionless variables defined by *Nicholson* [1983]:

$$\eta \equiv \frac{\gamma_e T_e + \gamma_i T_i}{T_e} \tag{6}$$

$$\tau \equiv \frac{2\eta}{3}\frac{m_e}{m_i}\omega_{pe}t \tag{7}$$

$$z \equiv \frac{2}{3}\left(\frac{\eta m_e}{m_i}\right)^{1/2}\frac{x}{\lambda_D} \tag{8}$$

$$E \equiv \frac{1}{\eta}\left(\frac{m_e}{m_i}\right)^{1/2}\left(\frac{3E_L^2}{64\pi n_e T_e}\right)^{1/2} \tag{9}$$

$$n \equiv \left(\frac{3m_i}{4\eta m_e}\right)^{1/2}\left(\frac{\delta n}{n_e}\right), \tag{10}$$

where γ_e and γ_i are the specific heat ratios of electrons and ions, respectively. The solutions of equations (4) and (5) can be found in terms of envelope solitons moving with constant speeds $V \leq V_g$, where V_g is the group velocity of the Langmuir waves. Several authors [see, *Rudakov*, 1973; *Kingsep, Rudakov and Sudan*, 1973; *Nishikawa, Hojo and Mima*, 1974; *Schamel, Yu and Shukla*, 1977; *Kuznetsov, Rubenchik and Zakharov*, 1986] have obtained the envelope soliton solutions by solving equations (4) and (5) under different approximations. These authors either have neglected the ion temperatures, i.e., $T_i \sim 0$, or have solved the nonlinear Schrodinger equation (obtained by neglecting the first term in equation (5)) for stationary solitons. In this paper, our motivation is to obtain the soliton solutions for realistic solar wind conditions and compare them with observations. The Mach number of the envelope soliton is defined as:

$$M = \frac{V}{c_s}, \tag{11}$$

where the ion sound speed c_s is defined as:

$$c_s^2 = \frac{\gamma_e T_e + \gamma_i T_i}{m_i}. \tag{12}$$

Without loss of generality, one can take $\gamma_e = 1$ and $\gamma_i = 5/2$.

The solutions for equations (4) and (5) can be written as:

$$E = E(\xi)\exp(-i\phi(\tau,\xi)) \tag{13}$$

$$n = n(\xi), \tag{14}$$

where $\xi = z - M\tau$ and ϕ is the phase of the envelope. Because, these are the solutions of solitons moving with constant speeds V, the variables E and n depend only on $(z - M\tau)$ but not on the spatial coordinate, z and time, τ, separately. Equation (4) can be separated into imaginary and real parts:

$$-M\frac{\partial E}{\partial \xi} + \left[E\frac{\partial^2\phi}{\partial\xi^2} + 2\frac{\partial E}{\partial\xi}\frac{\partial\phi}{\partial\xi}\right] = 0 \tag{15}$$

and

$$-E\left[\frac{\partial\phi}{\partial\tau} - M\frac{\partial\phi}{\partial\xi}\right] - \left[\frac{\partial^2 E}{\partial\xi^2} - E(\frac{\partial\phi}{\partial\xi})^2\right] = nE. \tag{16}$$

¿From equation (15), the phase of the envelope can be obtained as:

$$\phi(\tau,\xi) = -\Omega\tau + \frac{M\xi}{2}, \tag{17}$$

where Ω is some constant frequency. By using $\partial^2/\partial\tau^2 \rightarrow M\partial^2/\delta\xi^2$ and $\partial^2/\partial z^2 \rightarrow \partial^2/\partial\xi^2$ in equation (5), we obtain

$$n = -\frac{E^2}{1 - M^2}. \tag{18}$$

By substituting n and $\phi(\tau,\xi)$ from equations (18) and (17) in equation (16), one obtains:

$$\frac{\partial^2 E}{\partial\xi^2} = -E\left[\Omega + \frac{M^2}{4}\right] - \frac{E^3}{1 - M^2}. \tag{19}$$

By integrating once, this equation becomes:

$$\left(\frac{\partial E}{\partial\xi}\right)^2 = -E^2\left[\Omega + \frac{M^2}{4} + \frac{E^2}{2(1 - M^2)}\right]. \tag{20}$$

Writing $E(\xi) = E_0\epsilon(\xi)$ and

$$\Omega = -\frac{M^2}{4} - \frac{E_0^2}{2(1 - M^2)}, \tag{21}$$

equation (20) becomes

$$\left(\frac{\partial\epsilon(\xi)}{\partial\xi}\right)^2 = \frac{E_0^2}{2(1-M^2)}\epsilon(\xi)^2\left[1-\epsilon(\xi)^2\right]. \tag{22}$$

where E_0 is the normalized peak intensity of the envelope, and $\epsilon(\xi)$ is some auxiliary function. By making the change of variables

$$\xi = \frac{\sqrt{2(1-M^2)}}{E_0}\xi', \tag{23}$$

equation (22) becomes

$$\left(\frac{\partial\epsilon(\xi')}{\partial\xi'}\right)^2 = \epsilon(\xi')^2\left[1-\epsilon(\xi')^2\right]. \tag{24}$$

The solution of this equation, which decreases as $\xi' \to \pm\infty$ can be written as [*Tsytovich*, 1995]:

$$\epsilon = \cosh^{-1}\xi'. \tag{25}$$

Changing back to the original variables (equation 23), equation $E(\xi) = E_0\epsilon(\xi)\exp(-i\phi(\tau,\xi))$ becomes

$$E = E_0\cosh^{-1}\frac{E_0\xi}{\sqrt{2(1-M^2)}}\exp -i\left(\frac{M\xi}{2}-\Omega\tau\right). \tag{26}$$

Using equations (6) – (10), this soliton solution can be expressed as

$$E_L = E_{L0}\cosh^{-1}\left(\frac{x-Vt}{S}\right)\cos(\omega_N t - k_0 x), \tag{27}$$

where E_L is the amplitude of the envelope and E_{L0} is its peak amplitude. These envelope solitons can be stable for soliton speeds $V < (1/\sqrt{5})c_s$ [see, *Vladimirov et al.*, 1995].

Let us discuss the significance of each term in expression (27) in the light of the present observations. For example, ω_N is the nonlinear frequency shift, which is related to the observable parameters as:

$$\frac{\omega_N}{\omega_{pe}} = \frac{M^2}{2}\frac{\eta}{3}\frac{m_e}{m_i} - \frac{W_L}{8n_e T_e}. \tag{28}$$

For envelope solitons with speeds $V \sim V_g$, the nonlinear frequency shift becomes:

$$\frac{\omega_N}{\omega_{pe}} = \frac{3}{2} k_L^2 \lambda_D^2 - \frac{W_L}{8 n_e T_e}, \tag{29}$$

i.e., the nonlinear frequency shift ω_N is due to the dispersion (first term in (29)) as well as the ponderomotive effects (second term in (29)). These two effects oppose each other, i.e., have opposite signs. These types of nonlinear frequency shifts are very difficult to measure because they are too small (for example, in the case of a stationary solitons with $M \rightarrow 0$, $\omega_N/\omega_{pe} \simeq -W_L/8 n_e T_e$, which is $\simeq 10^{-6}$ for the events of the present study). The central wave number of the envelope soliton k_0 (equation 27) is defined as

$$k_0 = \frac{M}{3} \left(\frac{\eta m_e}{m_i} \right)^{1/2} \frac{1}{\lambda_D}, \tag{30}$$

i.e., $k_0 \sim k_L$ for $V = V_g$. The soliton width S is related to normalized peak energy as (equation (26)):

$$S = \left[\frac{3\eta}{1 - M^2} \frac{n_e T_e}{W_L} \right]^{1/2} \lambda_D. \tag{31}$$

i.e., $S \propto \lambda_D (W_L/n_e T_e)^{-1/2}$. This relationship between the soliton width and the peak energy density can be observationally verified. For example, in Table 2, the observed values of $W_L/(n_e T_e)$ and the 0.2-power widths $L_{0.2}$ of the broad peaks are given. In Figure 3 we plot the measured 0.2-power width of the broad peaks $L_{0.2}$ versus $(W_L/n_e T_e)^{1/2}$, which shows that higher the $(W_L/n_e T_e)^{1/2}$, narrower the width $L_{0.2}$. We calculate the correlation coefficient between these observed quantities as ~ 0.9. Thus, the observations agree very well with the expected scaling for Langmuir envelope solitons (equation 31). This implies that the Langmuir wave bursts captured by the FES instrument are most probably the fields trapped inside the self-generated density cavities.

We can also compute the predicted widths of envelope solitons using equation (31), since all the quantities on the right hand side (RHS) are measured except the Mach number M, which can be taken as $\sim 1/\sqrt{5}$ corresponding to the stable Langmuir

envelope solitons. For the measured temperatures of electrons (T_e) and ions (T_i) as given in Table 2, we obtain $\eta = (\gamma_e T_e + \gamma_i T_i)/T_e \sim 2.25, 1.33$ and ~ 1.37, for December 11, February 22, and March 7 events, respectively, where we have assumed $\gamma_e = 1$ and $\gamma_i = 5/2$. We denote the envelope soliton width, where the field is $0.2E_{L0}$ as $S_{0.2}$. Therefore, from equations (26) and (27), we obtain $\cosh^{-1}(S_{0.2}/S) = 0.2$ for $(S_{0.2}/S) = 2.29$, i.e., for t = 0 and $x \sim S_{0.2}$. By using this, we can write the 0.2-power width of the envelope soliton as:

$$S_{0.2} \sim 4\left(\frac{\eta}{1-M^2}\frac{n_e T_e}{W_L}\right)^{1/2}\lambda_D. \tag{32}$$

Thus, we obtain: $S_{0.2} \sim 6.7\,(n_e T_e/W_L)^{1/2}\lambda_D$, $\sim 5.1\,(n_e T_e/W_L)^{1/2}\lambda_D$, and $\sim 5.2\,(n_e T_e/W_L)^{1/2}\lambda_D$, for type III events of December, February and March, respectively, where we have used $M = V/c_s \sim 1/\sqrt{5}$. Using $(W_L/n_e T_e)$ and λ_D from Tables 2 and 1, we estimate the expected values of 0.2-power widths of envelope solitons $S_{0.2}$. The results are shown in Table 2 where the predicted value $S_{0.2}$ as well as the measured value $L_{0.2}$, are included. The $S_{0.2}$ and $L_{0.2}$ agree remarkably well, except, perhaps, for the second FES event of December 11 and first FES event of March 7 type III bursts. From Fig. 3, one can see that these two points lie well below the fitted line.

Using $L_{0.2}$ and the wavelengths of the Langmuir waves, we can also estimate the number of Langmuir waves trapped inside these envelope solitons. For example, the envelopes of December 11 contain 5, 3 and 4 Langmuir waves; the February 22 envelopes contain 3 and 5 waves; and the March 7 envelopes contain 2, 1, 2 and 2 waves, respectively. In terms of Debye lengths, λ_D, the widths of envelopes of December 11, February 22 and March 7 are equal to 1320, 790, 1230, 1160, 160, 710, 480, 830 and 730, respectively. Thus, we conclude that the observed broad field structures are Langmuir envelope solitons because the measured spatial scales are in excellent agreement with the predicted widths, $S_{0.2}$ and because of an excellent correlation between the $L_{0.2}$ and $(n_e T_e/W_L)^{1/2}$, as expected for envelope solitons.

3.2 Langmuir Solitons in a Weakly Magnetized Plasma

In the case of type III bursts, although the ambient magnetic field B is very weak, it guides the electron beam from inner solar atmosphere to several AU in the solar wind, thus the beam velocity $\vec{v_b}$ is almost parallel to the ambient magnetic field, $\vec{B}$. The weak magnetic field also determines the evolution of the beam excited Langmuir wave spectrum, which is forward peaked with a growth rate of (*Kaplan and Tsytovich*, 1973): $\gamma_b/\omega_{pe} = n_b/n_e(v_b/\Delta v_b)^2 \cos\theta$, where n_b and n_e are the electron densities of the beam and the ambient plasma, respectively, v_b is the beam speed, Δv_b is the spread in the beam speed and θ is the angle between $\vec{v_b}$ and $\vec{k_L}$. Since this growth peaks at $\theta \sim 0$, the initial spectrum of beam excited Langmuir waves is one-dimensional in nature.

When the ambient magnetic field is taken into account, the dispersion relation of Langmuir waves becomes:

$$\omega_L = \omega_{pe}\left(1 + \frac{3}{2}k_L^2\lambda_{De}^2 + \frac{\Omega_e^2}{2\omega_{pe}^2}\frac{k_\perp^2}{k_L^2}\right), \tag{33}$$

where $k_\perp$ is the component of the wave vector perpendicular to the ambient magnetic field. In the static approximation, the envelope equation for the amplitude of the magnetized Langmuir waves in dimensionless variables has the form [*Dysthe et al.*, 1978]:

$$\epsilon_\parallel \frac{\partial^2\Psi}{\partial z^2} + \frac{\partial^4\Psi}{\partial z^4} + \epsilon_\perp \nabla_\perp^2 \Psi + \frac{\partial}{\partial z}\left(\left|\frac{\partial\Psi}{\partial z}\right|^2 \frac{\partial\Psi}{\partial z}\right) = 0. \tag{34}$$

where Ψ is the envelope of Langmuir waves, $\epsilon_\parallel = 1 - \frac{\omega_{pe}^2}{\omega^2}$ and $\epsilon_\perp = 1 - \frac{\omega_{pe}^2}{(\omega^2-\Omega_e^2)}$. By a numerical method, a 'pancake' shaped soliton symmetric around an axis parallel to $\vec{B}$ is found for this equation by *Petviashvili* [1975]. He has shown that the thickness of this soliton is:

$$S = \lambda_D/(W_L/n_e T_e)^{1/2}, \tag{35}$$

whereas the radius of the pancake is

$$S_\perp = S(\Omega_e^2/\omega_{pe}^2)(S/\lambda_D). \tag{36}$$

Thus, in the early stage of soliton formation, as long as $\Omega_e^2/\omega_{pe}^2 >> k_L^2\lambda_D^2$, the transverse dimensions of the pancake-like solitons ($S_\perp$) are much larger than the longitudinal ones (S), forming highly anisotropic, elongated, dipole field structures. *Dysthe et al* [1978] have found an analytical one-dimensional soliton (planar) for equation (34) as:

$$E_L = E_{L0}\mathrm{sech}\left[S^{-1}\left(z \pm x\left(\frac{W_L/(n_eT_e) + 2\epsilon_{||}}{2|\epsilon_\perp|}\right)^{1/2}\right)\right]. \tag{37}$$

where S is the thickness of the pancake as given by equation (35), the local magnetic field is assumed to directed along z-axis. The stability of these solitons against the transverse perturbations has been studied by several authors [*Rowland*, 1985; *Kuznetsov, Rubenchik and Zakharov*, 1986; *Hadzievski et al.*, 1990; *Hadzievski and Skoric*, 1991]. The linear growth rate of the soliton instability is [*Kuznetsov, Rubenchik and Zakharov*, 1986; *Hadzievski et al.*, 1990]:

$$\gamma/\omega_{pe} = 2\left[\frac{W_L}{n_eT_e}[12 - 7\zeta(3)] - \frac{21}{4}\zeta(3)\frac{\Omega_e^2}{\omega_{pe}^2}\right]k_\perp^2\lambda_D^2, \tag{38}$$

where $\zeta(x) = \Sigma_n n^{-x}$ is Riemann's zeta function. This shows that a strong enough magnetic field B with

$$\frac{\Omega_e^2}{\omega_{pe}^2} > 0.43\frac{W_L}{n_eT_e} \tag{39}$$

can stabilize the linear instability. However, *Hadzievski et al* [1990] have shown that the instability reappears if one takes into account the next term in the expansion in transverse wave numbers $k_\perp$, and Langmuir collapse will ensue.

As discussed by *Krasnoselskikh and Sotnikov* [1977], even though for $\Omega_e/\omega_{pe} >> k_L\lambda_D$, the transverse dimension of the planar soliton $S_\perp$ is larger than the longitudinal one S, and $S_\perp$ will decrease rapidly in comparison with S, until the solitons become isotropic. Thus, the Fast Envelope Sampler appears to capture the solitons at this isotropic stage of their evolution when $k_L\lambda_D$ is approaching Ω_e/ω_{pe}, and the solitons evolve independently of the local magnetic field. These solitons should collapse eventually. These observations do not confirm the simulation results of *Hadzievski et al.*

[1990], which showed that the form of the cavities and trapped energy depend on the magnetic field strength.

If the soliton conserved energy, *Krasnoselskikh and Sotnikov* [1977] showed that they could not construct a self-similar solution to collapse in a magnetic field. If the soliton radiated away the electrostatic energy, however, they could get such a solution. *Rowland* [1985], using computer simulations, showed that if $W_L/(n_eT_e) < (\Omega_e/\omega_{pe})^2$, planar solitons with a finite transverse scale would radiate the wave energy before collapsing. This agreed with the earlier theory of *Krasnoselskikh and Sotnikov* [1977]. This process is termed as weak collapse by *Kuznetsov and Turitsyn* [1990] and *Hadzievski et al* [1990]. When the most of the energy is absorbed by the electrons, the collapse process is called strong collapse [*Kuznetsov*, 1996].

4. Discussion

We have analyzed the $\sim$ 1 millisecond observations of the Langmuir waves which form broad intense peaks with spatial scales ranging from 480 to 1320 λ_D. Our analysis indicates that the peak intensities of these envelopes exceed the threshold for modulational or OTSI instabilities. The widths of these broad Langmuir field structures correlate well with $(n_eT_e/W_L)^{1/2}$, as expected for envelope solitons. This implies that the density cavities associated with these solitons are most probably generated by the Langmuir waves themselves due to their ponderomotive force. The predicted widths of envelope solitons calculated using the observed intensities of the broad Langmuir field structures agree remarkably well with the observed widths. These findings strongly suggest that the broad Langmuir wave peaks correspond to envelope solitons generated by the modulational or oscillating two stream instabilities. This implies that strong turbulence processes play a significant role in the stabilization of the electron beams which generate the Langmuir waves.

In earlier work [*Thejappa et al.*, 1993a], we discussed the role of the electrostatic

decay instability which is a weak turbulence process in the development of type III bursts. During this process, the beam-excited Langmuir waves are expected to decay into daughter Langmuir waves and ion acoustic waves. As shown in *Thejappa et al.*, [1993a], the threshold condition for electrostatic decay is satisfied for all broad peaks shown in Figure 2, implying that this process should co-exist with strong turbulence processes in the source regions of some of the type III events. One can estimate the maximum possible Doppler-shifted frequencies f_s for the daughter ion acoustic waves by using the relation: $f_s \simeq k_s(V_{sw} + c_s)/(2\pi)$, where $k_s \simeq 2k_L$ is the wave number of the ion acoustic waves. Using the observed values of V_{sw}, c_s and k_L (see, Table 1), we obtain the predicted values for f_s as 99.3 Hz, 69.2 Hz, and 86 Hz for the Dec. 11, Feb. 22 and March 7 events, respectively. One can also estimate the expected ion acoustic electric field values, E_s, by using the energy conservation arguments. In the present case, E_s values lie in the range $(1.4 - 3.8) \times 10^{-5}$ Vm^{-1}, $(5.3 - 6.7) \times 10^{-6}$ Vm^{-1} and $(0.9 - 2.7) \times 10^{-5}$ Vm^{-1} for the events of Dec. 11, Feb. 22, and March 7. In our previous study, we failed to find any electric field enhancements which might correspond to these predicted ion acoustic wave signals. We therefore concluded that although threshold conditions were satisfied, the electrostatic decay process was not evident.

In this study, rather than using the time profiles as in *Thejappa et al.* [1993a], we analyzed the spectral data of peak electric fields obtained by the WFA during 1 to 2 minute intervals covering the FES events. In Figures 4a, b and c, we present the low frequency electric field spectra from WFA as well as the high frequency spectra from the PFR. It is clear from these plots that for most of the cases, the low frequency electric field spectra show weak enhancements at $\sim$ 100 Hz coincident with the passage of modulationally unstable solitons. We interpret these simultaneous occurrences of low frequency electric field signals and Langmuir waves as evidence of the coexistence of weak and strong turbulence processes in the type III burst source region [*Thejappa and MacDowall*, 1998]. This suggests that during some type III events the electrostatic decay

instability can remove Langmuir waves from resonance with electron beams. This leads to the accumulation of Langmuir waves at long wavelengths, forming the so-called weak turbulence Langmuir condensate, which eventually becomes modulationally unstable.

There are at least two reasons for not detecting low frequency wave enhancements in association with solitons for some of the events. First, the size of the solitons is $\leq$ 40 km, well below the coherence length of $v_b/\gamma_L \geq$ 1000 km. Therefore, the resonances required by weak turbulence processes cannot occur. Second, the threshold for electrostatic decay is at least two orders of magnitude greater than that for modulational instability (see Sec. 4), thus electrostatic decay should not be excited, at least until the modulational instability has saturated.

High frequency ion acoustic-like waves [*Gurnett and Frank*, 1978] can play the role of small scale ($k_s >> k_L$) density fluctuations: which can cause the nonresonant anomalous absorption of Langmuir waves due to scattering [*Goldman and DuBois*, 1982; *Russell and Goldman*, 1983]. This can also stabilize the electron beam. The observed lack of high frequency ion acoustic-like noise between 0.5 to 3 kHz during intervals of intense Langmuir wave activity was interpreted in terms of this process. As shown previously [*Thejappa et al.* 1993a], the ion acoustic-like waves are not associated preferentially with Langmuir waves, i.e., Langmuir wave growth is not suppressed by scattering on density fluctuations associated with high frequency ion acoustic-like waves. This implies that anomalous scattering of Langmuir waves by small scale density fluctuations is probably not a significant stabilization mechanism for type III burst exciters.

5. Conclusions

Using Ulysses data from the URAP experiment we have presented observational evidence for the Langmuir envelope solitons, generated by the modulational instability or OTSI in the source regions of solar type III radio bursts. The high time resolution observations show that the type III associated Langmuir waves occur as broad intense

peaks with time scales ranging from $15 - 90$ ms (equivalent to the spatial scales of $6 - 27$ km). We have identified the broad peaks as Langmuir envelope solitons based on: (1) W_L/n_eT_e of the broad Langmuir peaks are well above the modulational instability threshold of $\sim 10^{-5}$, (2) the spatial scales of these localized field structures, which range from 1 to 5 Langmuir wavelengths, show a high degree of inverse correlation with $(W_L/n_eT_e)^{1/2}$, as expected of envelope solitons, and (3) the observed widths of these broad peaks agree very well with the predicted widths of envelope solitons calculated using the observed values W_L/n_eT_e and other solar wind parameters. These observations support the view that strong turbulence processes, namely the modulational instability or OTSI, are the means by which some of the type III electron beams are stabilized.

In some cases, low frequency electric fields show weak spectral enhancements at $\sim$ 100 Hz, perhaps corresponding to long wavelength ion acoustic waves. The close association of these waves with the modulationally unstable Langmuir solitons, indicate that the electrostatic decay instability coexists with the modulational instability in certain type III burst source regions.

Acknowledgments. The URAP investigation is a collaboration of NASA Goddard Space Flight Center, Observatoire de Paris-Meudon, the University of Minnesota, and the Centre d'etudes des Environnements Terrestre et Planetaires (CETP). We thank P. Kellogg for invaluable contributions. We acknowledge A. Balogh and D. McComas for making other Ulysses data sets available through the NSSDC. The research of GT is supported by the NASA grants NAG57145, NCC-255 and NAG56059.

References

Balogh, A. et al., The magnetic field investigation on the Ulysses mission: Instrumentation and preliminary scientific results, *Astron. Astrophys. Suppl. ser.*, *92*, 221, 1992.

Bame, S. J. et al., The Ulysses solar wind plasma experiment, *Astron. Astrophys. Suppl. Ser.*, *92*, 237, 1992.

Bohm, D., and E. P. Gross, Theory of plasma oscillations, A, Origin of medium-like behavior, *Phys. Rev.*, *75*, 1851, 1949.

Degtyarev, L. M., V. G. Nakhan'kov and L. I. Rudakov, Dynamics of the formation and interaction of Langmuir solitons and strong turbulence, *Sov. Phys. JETP.*, *40*, 264, 1974.

Dysthe, K. B., E. Mjolhus, H. L. Pecseli, and L. Stenflo, Langmuir solitons in magnetized plasmas, *Plasma Phys.*, *20*, 1087, 1978.

Ergun, R. E., et al., Wind spacecraft observations of solar impulsive electron events associated with solar type III radio bursts, *Astrophys. J.*, *503*, 435, 1998.

Goldman, M. V. and D. F. DuBois, Beam-plasma instability in the presence of low-frequency turbulence, *Phys. Fluids*, *25*, 1062, 1982.

Goldstein, M. L., R. A. Smith and K. Papadopoulos, Nonlinear stability of solar type III radio bursts, II. Application to observations near 1 AU, *Astrophys. J.*, *237*, 683, 1979.

Gurnett, D. A. and L. A. Frank, Ion acoustic waves in the solar wind, *J. Geophys. Res.*, *83*, 58, 1978.

Hadzievski,Lj. R., M. M. Skoric, A. M. Rubenchik, E. G. Shapiro, and S. K. Turitsin, Langmuir soliton stability and collapse in a weak magnetic field, *Phys. Review A.*, *42*, 3561, 1990.

Hadzievski,Lj. R., and M. M. Skoric, On transverse instability of large-amplitude Langmuir solitons, *Phys. Fluids, B*, *3*, 2452, 1991.

Kaplan, S. A., and V. N. Tsytovich, *Plasma Astrophysics*, Pergamon Press (Oxford), 1973.

Kellogg, P. J., K. Goetz, R. L. Howard, R. L. and S. Monson, Evidence for Langmuir wave collapse in the interplanetary plasma, *J. Geophys. Res. Letters*, *19*, 1303, 1992.

Kingsep, A. S., L. I. Rudakov, and R. N. Sudan, Spectra of strong Langmuir turbulence, *Phys. Rev. Lett.*, *31*, 1483, 1973.

Krasnoselskikh, V. V. and V. I. Sotnikov, Plasma wave collapse in a magnetic field, *Sov. J. Plasma Phys.*, *3*, 491, 1977.

Kuznetsov, E. A., A. M. Rubenchik, and V. E. Zakharov, Soliton stability in plasmas and hydrodynamics, *Phys. Reports*, *142*, 103, 1986.

Kuznetsov, E. A., Wave collapse in plasmas and fluids, *CHAOS*, *6*, 381, 1996.

Kuznetsov, E. A., and S. K. Turitsyn, Quasiclassical Langmuir wave collapse in a magnetic field, *Sov. J. Plasma Phys.*, *16*, 524, 1990.

Lin, R. P., W. K. Levedahl, W. Lotko, D. A. Gurnett, and F. L. Scarf, Evidence for nonlinear wave-wave interactions in solar type III radio bursts, *Astrophys. J.*, *308*, 954, 1986.

Nicholson, D. R., *Introduction to Plasma Theory*, (New York: John Wiley & Sons), 1983.

Nicholson, D. R., M. V. Goldman, P. Hoyang, and J. C. Weatherall, Nonlinear Langmuir waves during type III solar radio bursts, *Astrophys. J.*, *223*, 605, 1978.

Nishikawa, K., H. Hojo, and K. Mima, Coupled nonlinear electron-plasma and ion acoustic waves, *Phys. Rev. Lett.*, *33*, 148, 1974.

Papadopoulos, K., M. L. Goldstein and R. A. Smith, Stabilization of electron streams in type III solar radio bursts, *Astrophys. J.*, *190*, 175, 1974.

Petviashvili, V. I., Three-dimensional solitons of extraordinary and plasma waves, *Sov. J. Plasma Phys.*, *1*, 15, 1975.

Reiner, M. J., J. Fainberg and R. G. Stone, Detection of fundamental and harmonic type III radio emission and associated Langmuir waves at the source region, *Astrophys. J.*, *394*, 340, 1992.

Robinson, P. A., Nonlinear wave collapse and strong turbulence, *Rev. Mod. Phys.*, *69*, 507, 1997.

Rowland, H. L., Strong Langmuir turbulence in a magnetic field, *Phys. Fluids*, *28*, 190, 1985.

Rudakov, L. I., Deceleration of electron beams in a plasma with a high level of Langmuir turbulence, *Sov. Phys. Dokl.*, *17*, 1166, 1973.

Russell, D. A. and M. V. Goldman, Backscattering cascade of beam modes off ambient density

fluctuations, *Phys. Fluids*, *26*, 2717, 1983.

Sagdeev, R. Z., The 1976 Oppenheimer lectures: Critical problems in plasma astrophysics. I. Turbulence and nonlinear waves, *Rev. Mod. Phys.*, *51*, 1, 1979.

Schamel, H., M. Y. Yu, and P. K. Shukla, Finite amplitude envelope solitons, *Phys. Fluids*, *20*, 1286, 1977.

Shapiro, V. D., and V. I. Shevchenko, Strong turbulence of plasma oscillations, *Handbook of Plasma Physics*, Eds., M. N. Rosenbluth and R. Z. Sagdeev, Vol. 2: *Basic Plasma Physics II.* edited by A. A. Galeev and R. N. Sudan, 1984.

Smith, R. A., M. L. Goldstein and K. Papadopoulos, Nonlinear stability of solar type III radio bursts, I. Theory, *Astrophys. J.*, *234*, 348, 1979.

Stone, R. G., et al., The Unified radio and plasma wave investigation, *Astron. Astrophys. Suppl. Ser.*, *92*, 291, 1992.

Sturrock, P. A., 1964, in *Proceedings of AAS- NASA Symposium on the Physics of Solar Flares*, W. N. Hess, eds. (NASA SP-50), p.357.

Thejappa, G., D. Lengyel-Frey, R. G. Stone and M. L. Goldstein, Evaluation of emission mechanisms at ω_{pe} using Ulysses observations of type III bursts, *Astrophys. J.*, *416*, 831, 1993a.

Thejappa, G., D. Lengyel-Frey, R. G. Stone and M. L. Goldstein, Evaluation of solar type III burst theories using Ulysses URAP observations, *in Theoretical Geoplasma Physics*, edited by Tom Chang, MIT, p.517, 1993b.

Thejappa, G., D. G. Wentzel and R. G. Stone, Low-frequency waves associated with Langmuir waves in solar wind, *J. Geophys. Res.*, *100*, 3417, 1995.

Thejappa, G., R. G. Stone and M. L. Goldstein, Detection of Langmuir solitons: Implications for type III burst emission mechanisms at $2\omega_{pe}$, *Astrophysics and Space Sci.*, *243*, 195, 1996.

Thejappa, G., and R. J. MacDowall, Evidence for strong and weak turbulence processes in the source region of a local type III radio burst, *Astrophys. J.*, *498*, 465, 1998.

Thiessen, J. P. and P. J. Kellogg, Langmuir wave decay and collapse in the Jovian foreshock, *Planet. Space. Sci.*, *41*, 823, 1993.

Tsytovich, V. N., *Nonlinear Effects in Plasma* (New York: Plenum), 1970.

Tsytovich, V. N., *Lectures on Non-linear Plasma kinetics*, Spinger-Verlag, Berlin, 1995.

Vladimirov, S. V., V. N. Tsytovich, S. I. Popel, F. Kh. Khakimov, *Modulational Interactions in Plasmas*, Kluwer Academic Publishers, Boston, 1995.

Zakharov, V. E., Collapse of Langmuir waves, *Sov. Phys. JETP. 35*, 908, 1972.

Received _____

Figure 1. Time profiles of the electric field components corresponding to the harmonic and fundamental local type III solar radio bursts and the corresponding Langmuir waves. The columns 1, 2 and 3 correspond to 11 December 1990, 22 February 1991 and 7 March 1991, respectively. The first and second rows correspond to type III bursts at second harmonic and the fundamental of the electron plasma frequency, f_{pe}, and the third row corresponds to Langmuir waves.

Figure 2. High time resolution observations of Langmuir waves observed during the type III burst events of (a) 11 December 1990, (b) 22 February 1991, and (c) 7 March 1991. These measurements were taken with a wide band (6-60 kHz) filter, and 1.12 msec time resolution. The enhanced background level after about 600 ms in many of the panels was caused by the switch-on of the 32 dB attenuator. Narrow intense spikes observed on top of the central broad peaks of the Dec. 11 and March 7 events have been removed from the data. The broad central peaks seen on all three days satisfy the conditions expected of envelope solitons.

Figure 3. Observed 0.2-power width $L_{0.2}$ of the broad FES peaks versus $(n_e T_e)/W_L)^{1/2}$. Here the $L_{0.2}$ is calculated using the relation, $L_{0.2} = t_{0.2} \times V_{sw}$, where $t_{0.2}$ is the 0.2-power duration of the broad peaks and V_{sw} is the solar wind speed as given in Table 1, n_e and T_e are the electron density and temperatures, respectively and W_L is the peak energy density of the broad FES peaks. The correlation coefficient in this case is 0.9.

Figure 4. Spectral plots of electric fields observed by the WFA and PFR during 1- or 2-minute intervals covering the high time resolution snapshots of Fig. 2. The dotted line corresponds to instrumental threshold. The spectral peak in these figures at $\sim 10^4$ Hz corresponds to Langmuir waves.

Table 1. Summary of the observed solar wind parameters during the type III events of the present study. Col. 1 gives the date of type III event; col. 2, the observed electron density, n_e in m^{-3}, col. 3, the observed electron plasma frequency, f_{pe} in kHz, col. 4, the observed magnetic field, B in units of nT, col. 5, $(\Omega_e/\omega_{pe})^2$, where Ω_e and ω_{pe} are the electron cyclotron and electron plasma frequencies, respectively, col. 6, the average electron temperature, T_e, col. 7, the average ion temperature, T_i, col. 8, the Debye length λ_D in meters, col. 9 gives the solar wind speed, V_{sw} in km/s, and col. 10 gives the sound speed, c_s in km/s.

Event	n_e	f_{pe}	B	$(\Omega_e/\omega_{pe})^2$	T_e	T_i	λ_D	V_{sw}	c_s
Dec. 11	1.7×10^6	11.6	6	2×10^{-4}	10^5	5×10^4	17	382	45
Feb. 22	1.3×10^6	10.2	2	3×10^{-5}	7.6×10^4	10^4	17	310	30
March 7	1.3×10^6	10.2	2	3×10^{-5}	4.7×10^4	7×10^3	13	401	21

Table 2. Summary of the high time resolution observations of Langmuir waves. Here E_L is the observed peak electric field corresponding to the broad central peaks in units of V/m and $W_L/(n_eT_e)$ are the corresponding normalized energy densities. The $t_{0.2}$ is the measured 0.2-power duration of the broad central peak in units of ms and the $L_{0.2}$ is the corresponding width, calculated using the formula: $L_{0.2} = t_{0.2} \times V_{sw}$, where V_{sw} is the solar wind speed as given in Table 2. The col. (3-6) correspond to the respective FES events of the present study. The $S_{0.2}$ is the predicted spatial scale of the envelope soliton

Dec. 11, 1990	E_L (V/m)	3.3×10^{-3}	3.2×10^{-3}	3.3×10^{-3}	—
	$\frac{W_L}{n_eT_e}$	2×10^{-5}	1.9×10^{-5}	2×10^{-5}	—
	$t_{0.2}$ (ms)	58.4	35.1	54.5	—
	$L_0.2$ (km)	22.3	13.4	20.8	—
	$S_{0.2}$ (km)	21.2	21.8	21.2	—
Feb. 22, 1991	E_L V/m	2.3×10^{-3}	1.8×10^{-3}	—	—
	$\frac{W_L}{n_eT_e}$	1.7×10^{-5}	1.0×10^{-5}	—	—
	$t_{0.2}$ (ms)	62.3	85.7	—	—
	$L_{0.2}$ (km)	19.3	26.6	—	—
	$S_{0.2}$ (km)	22.7	29.6	—	—
Mar 7, 1991	E_L V/m	2.3×10^{-3}	4.6×10^{-3}	3×10^{-3}	3.4×10^{-3}
	$\frac{W_L}{n_eT_e}$	2.8×10^{-5}	1.0×10^{-4}	4.7×10^{-5}	6×10^{-5}
	$t_{0.2}$ (ms)	23.4	15.6	27.3	23.4
	$L_{0.2}$ (km)	9.4	6.3	10.9	9.6
	$S_{0.2}$ (km)	12.97	6.9	10.01	8.9

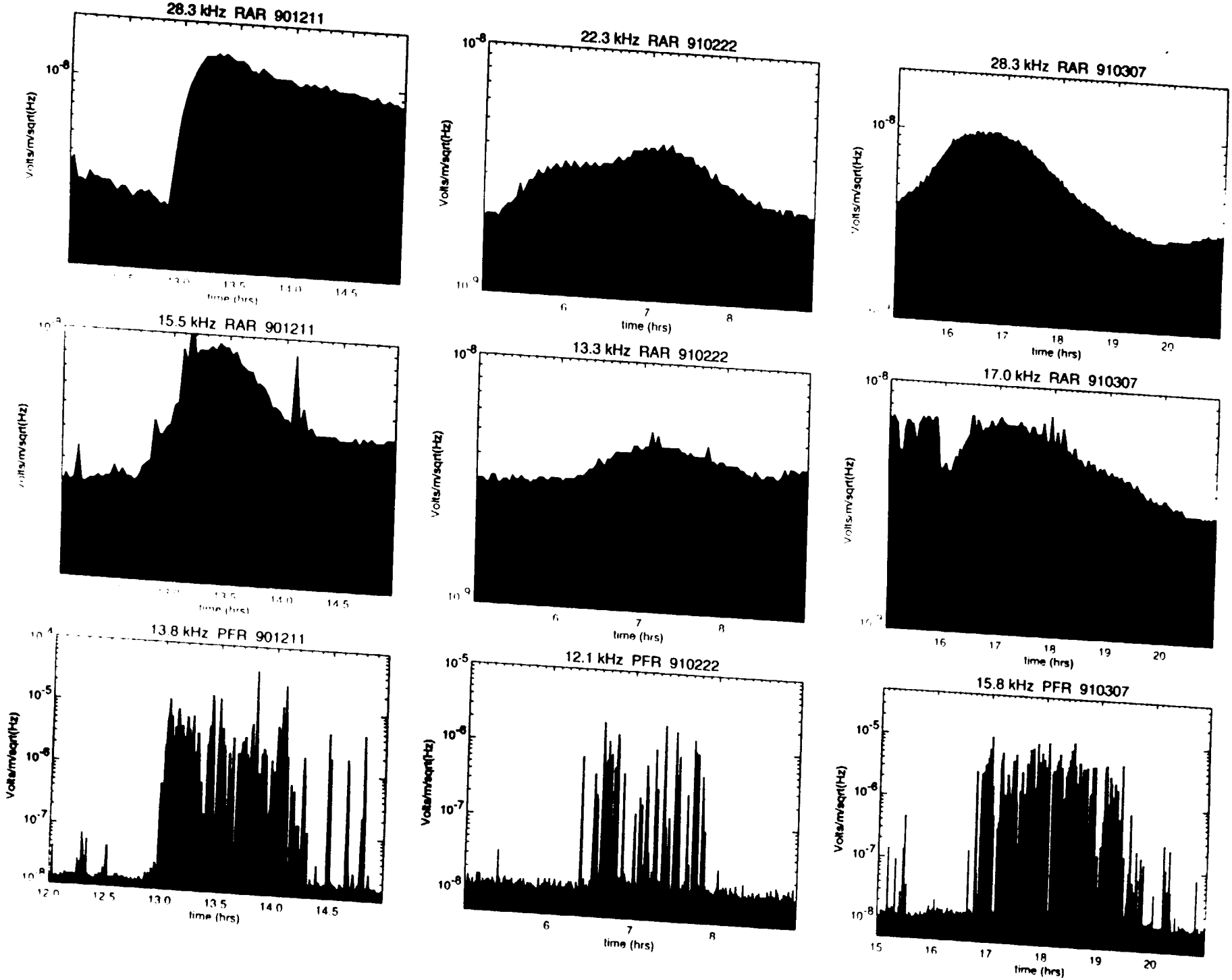
28.3 kHz RAR 901211
22.3 kHz RAR 910222
28.3 kHz RAR 910307
15.5 kHz RAR 901211
13.3 kHz RAR 910222
17.0 kHz RAR 910307
13.8 kHz PFR 901211
12.1 kHz PFR 910222
15.8 kHz PFR 910307
Volts/m/sqrt(Hz)
time (hrs)

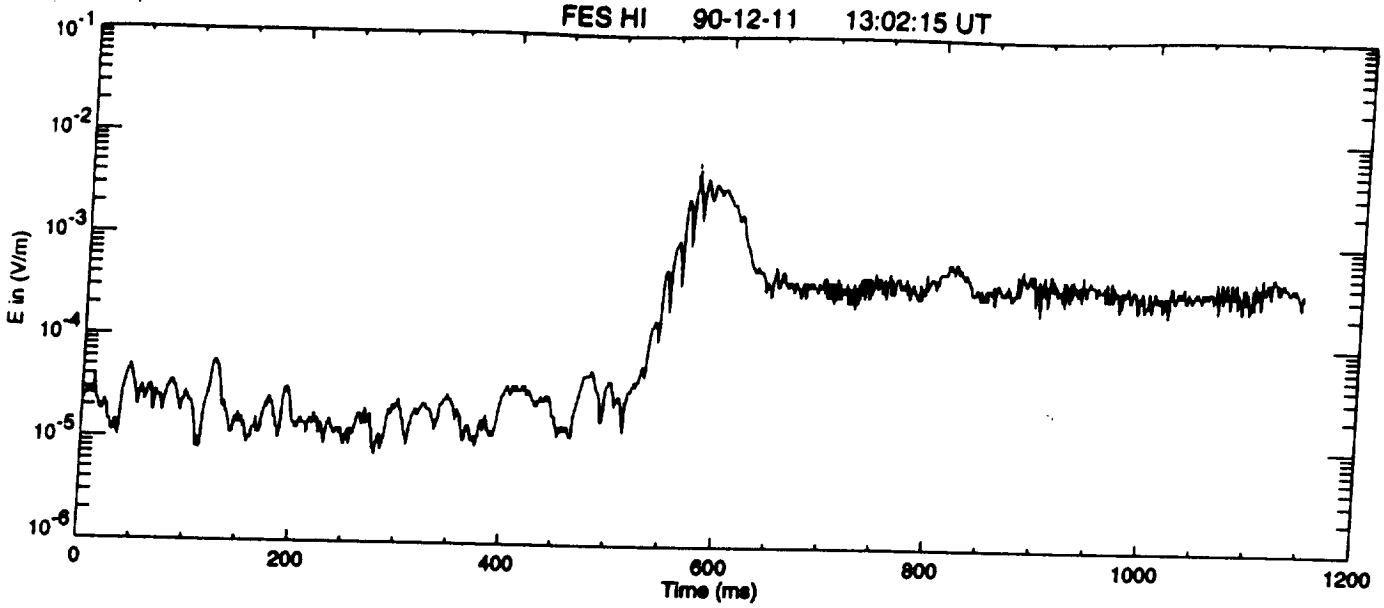
FES HI 90-12-11 13:02:15 UT
E in (V/m)
Time (ms)

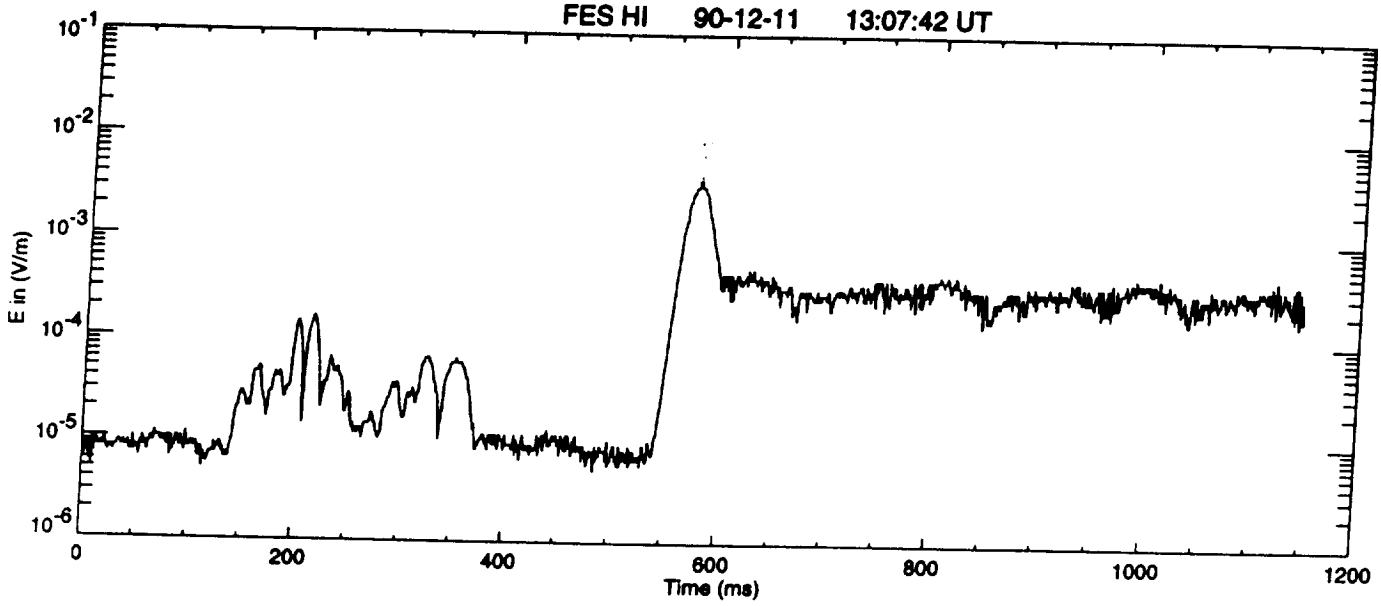
FES HI 90-12-11 13:07:42 UT
E in (V/m)
Time (ms)

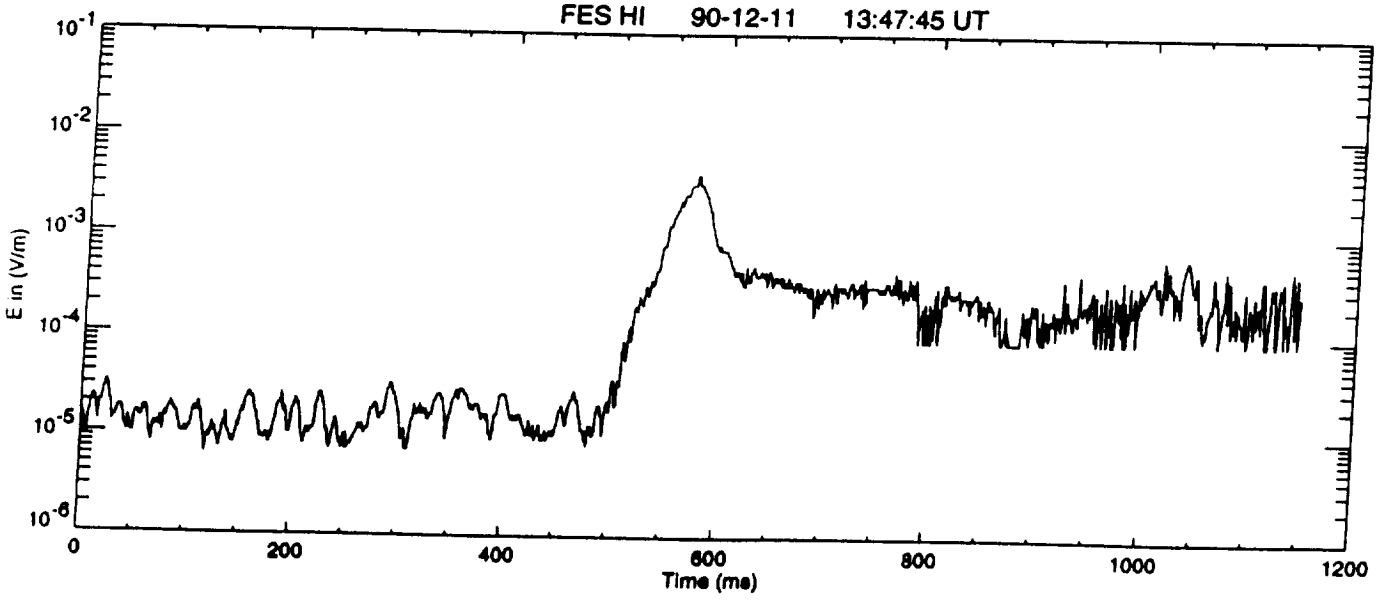
FES HI 90-12-11 13:47:45 UT
E in (V/m)
Time (ms)

Fig 2a

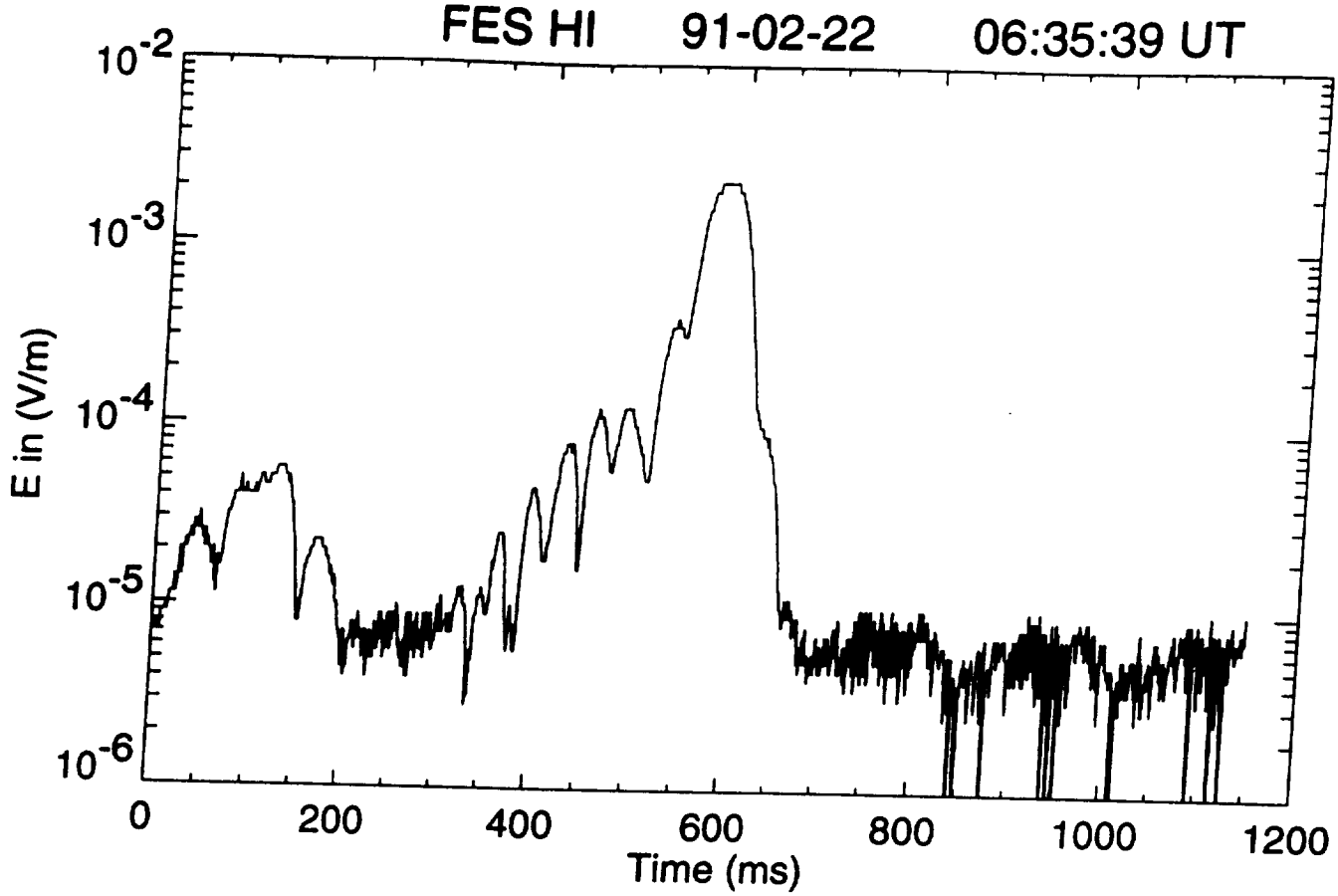
FES HI 91-02-22 06:35:39 UT
E in (V/m)
10-2
10-3
10-4
10-5
10-6
0
200
400
600
800
1000
1200
Time (ms)

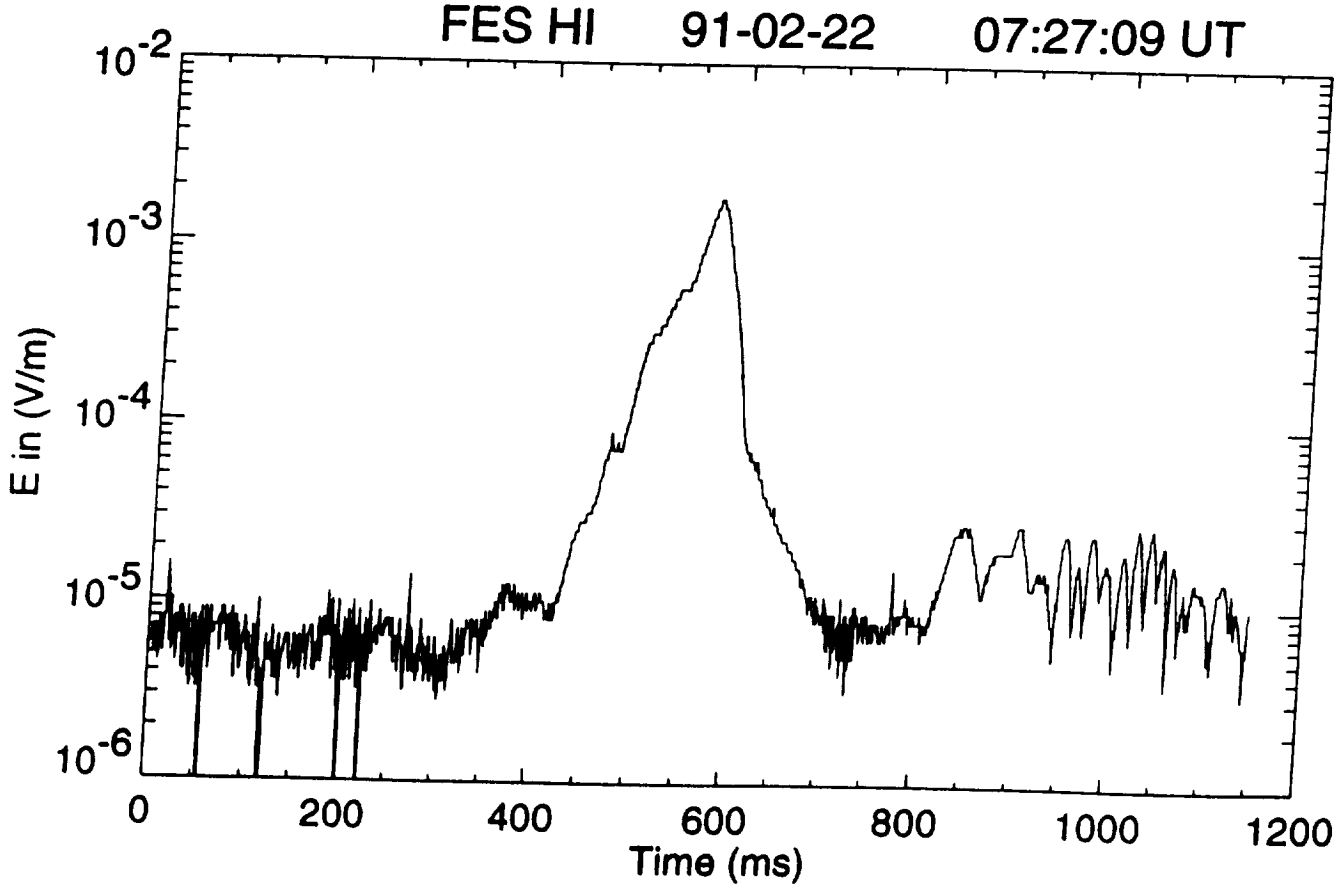
FES HI 91-02-22 07:27:09 UT
E in (V/m)
10-2
10-3
10-4
10-5
10-6
0
200
400
600
800
1000
1200
Time (ms)

Fig. 26

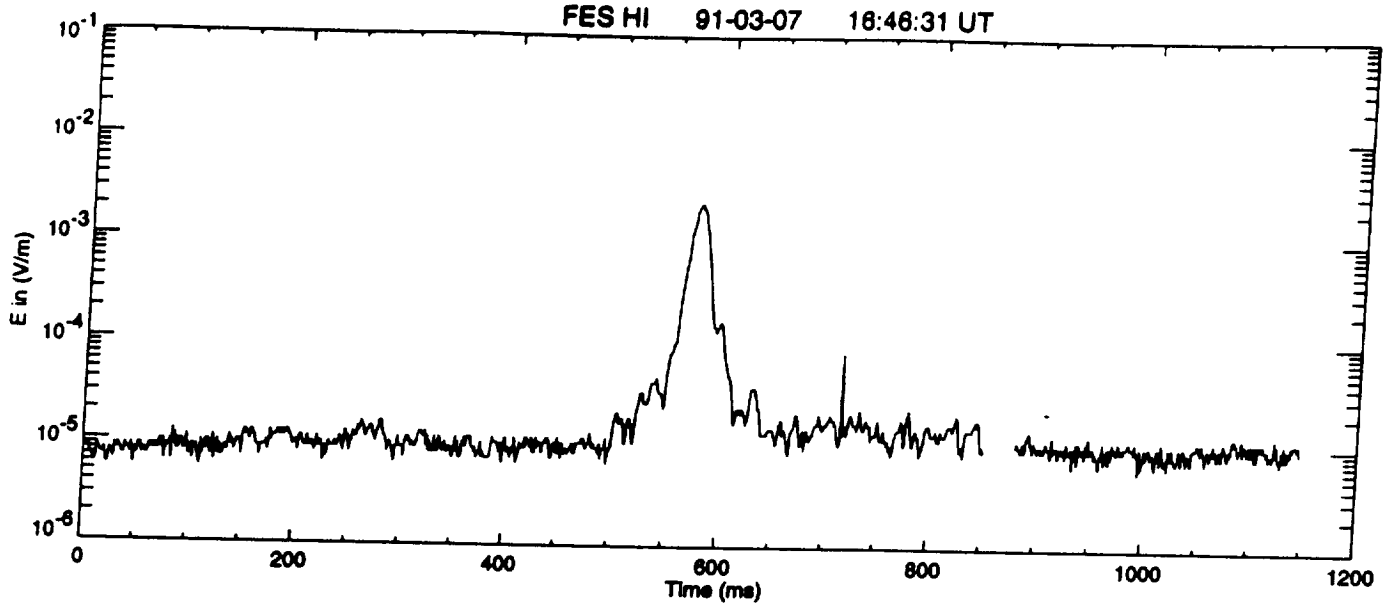
FES HI 91-03-07 16:46:31 UT
E in (V/m)
Time (ms)

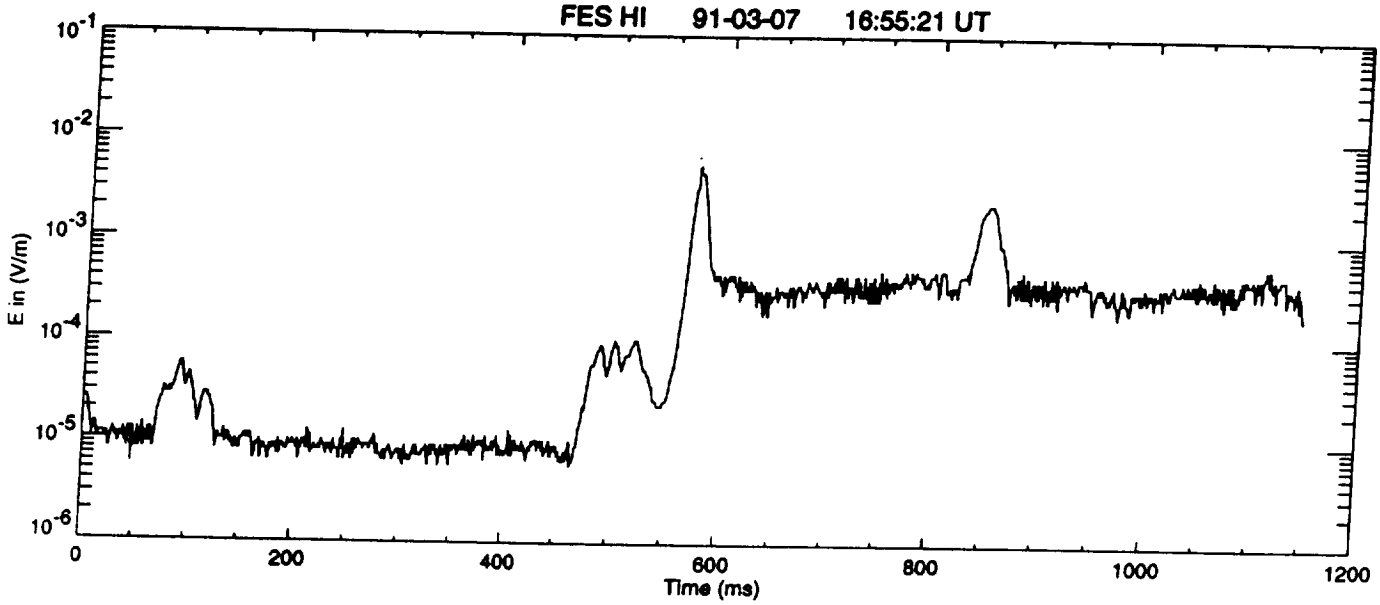
FES HI 91-03-07 16:55:21 UT
E in (V/m)
Time (ms)

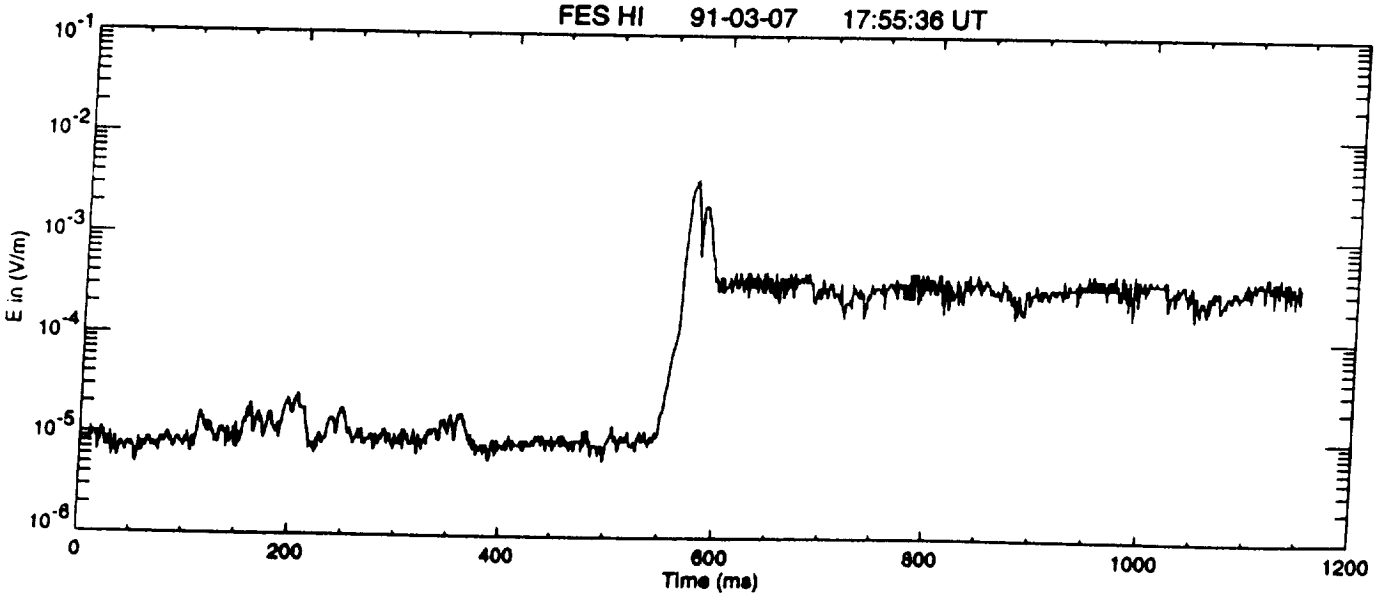
FES HI 91-03-07 17:55:36 UT
E in (V/m)
Time (ms)

Fig 2c

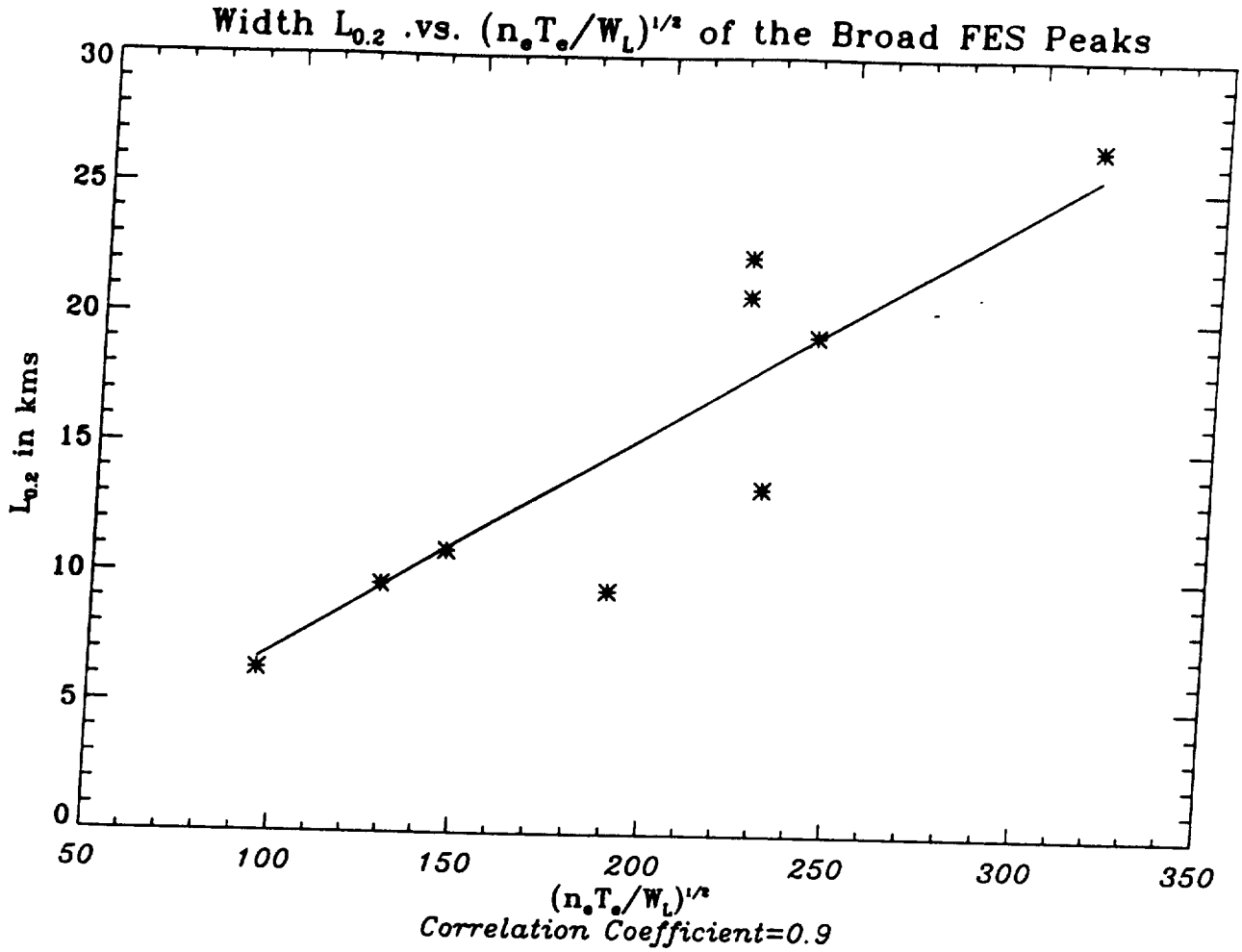
Width $L_{0.2}$ .vs. $(n_eT_e/W_L)^{1/2}$ of the Broad FES Peaks
$L_{0.2}$ in kms
30
25
20
15
10
5
0
50
100
150
200
250
300
350
$(n_eT_e/W_L)^{1/2}$
Correlation Coefficient=0.9

Fig. 3

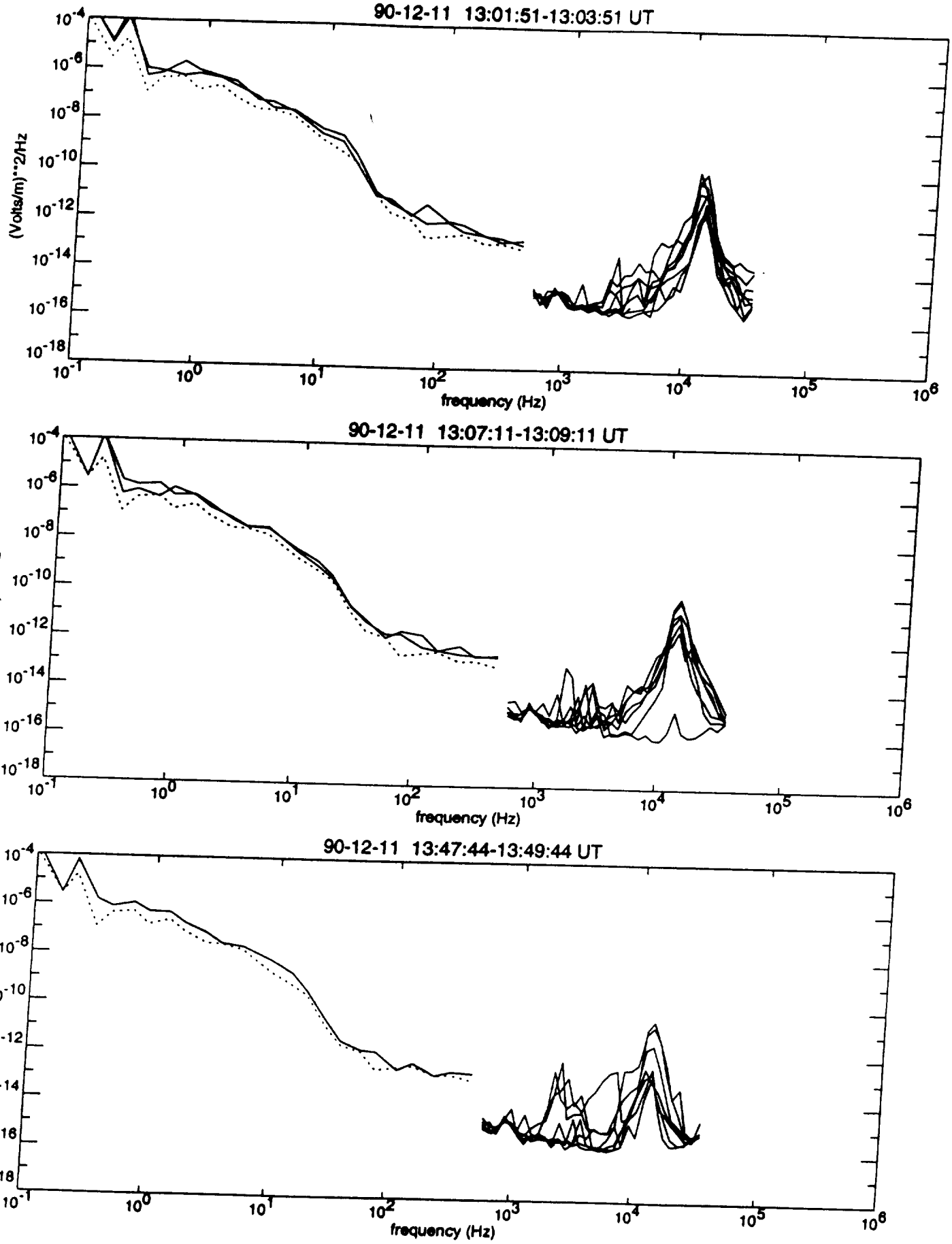
90-12-11 13:01:51-13:03:51 UT
90-12-11 13:07:11-13:09:11 UT
90-12-11 13:47:44-13:49:44 UT
(Volts/m)**2/Hz
frequency (Hz)

Fig. 4a

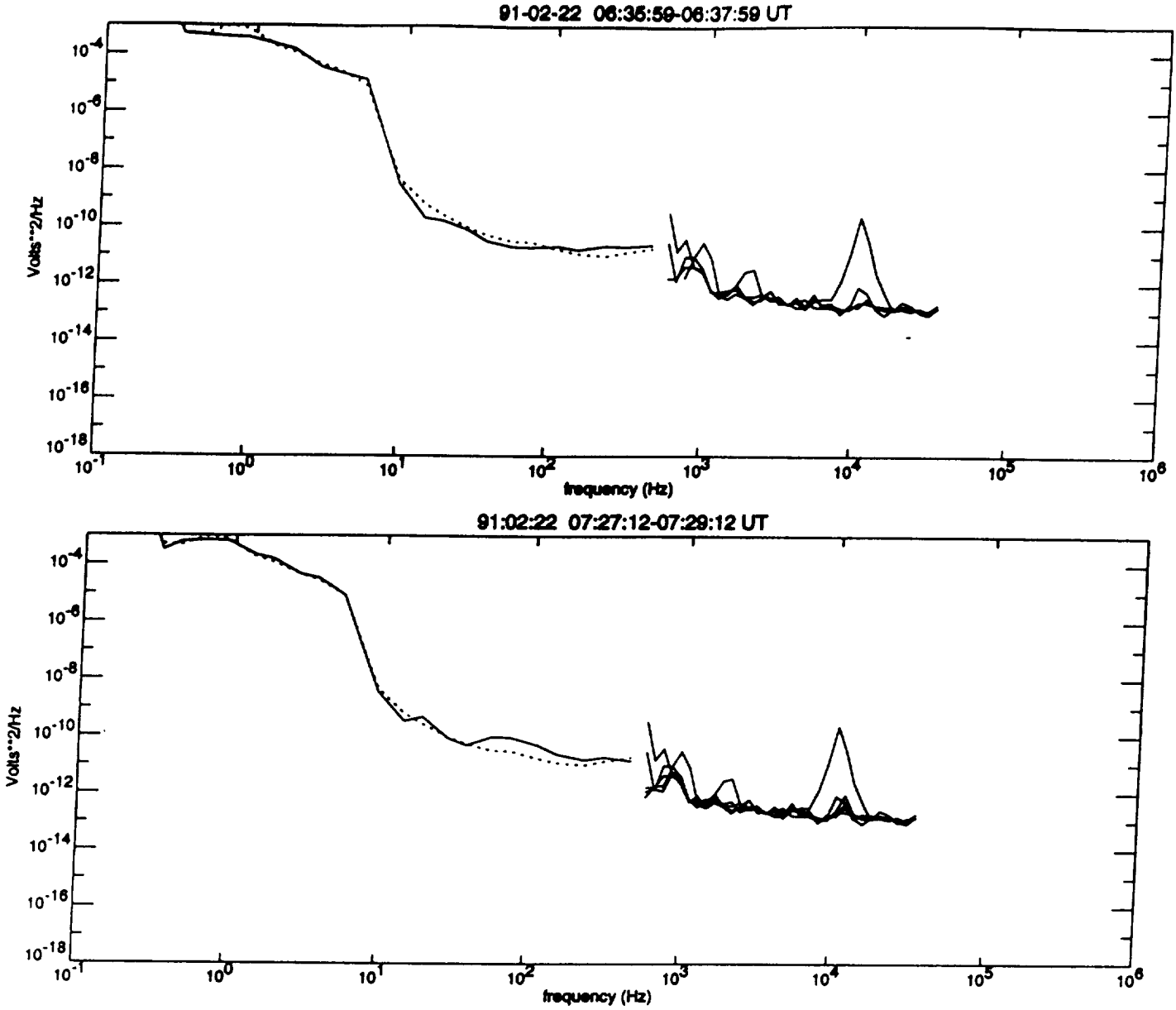
91-02-22 06:35:59-06:37:59 UT
Volts**2/Hz
frequency (Hz)
91:02:22 07:27:12-07:29:12 UT
Volts**2/Hz
frequency (Hz)

Fig. 46